Adaptive Dithering for Improved Dynamic Range in Mixed-Resolution ADC Digital Radars

Shaikh, M. A.; Joseph, G.; Pandharipande, A.; Myers, N. J.

DOI
10.1109/RadarConf2559087.2025.11205063

Publication date
2025

Document Version
Final published version

Published in
Proceedings of the 2025 IEEE Radar Conference, RadarConf 2025

Adaptive Dithering for Improved Dynamic Range in Mixed-Resolution ADC Digital Radars

Mohammed Aasim Shaikh[1], Geethu Joseph[1], Ashish Pandharipande[2], Nitin Jonathan Myers[1]
[1]Delft University of Technology, The Netherlands
[2]NXP Semiconductors, The Netherlands
{m.a.shaikh, n.j.myers, g.joseph}@tudelft.nl, ashish.pandharipande@nxp.com

***Abstract* — Digital radars with low-resolution analog-to-digital converters (ADCs) can reduce digital processing complexity and power consumption but suffer from limited dynamic range. The poor dynamic range causes high radar cross-section (RCS) targets to mask low-RCS ones. To mitigate this issue, we propose operating the ADC at a high resolution during the initial slow-time slot of each radar frame. The high-resolution measurements are used to estimate the range and RCS of dominant targets, which, along with their known Doppler statistics, are used to construct a dither signal. This dither signal is then employed to acquire low-resolution ADC measurements in the subsequent slow-time slots. With the proposed receiver architecture, our method suppresses strong target returns in the low-resolution measurements, effectively unmasking weak targets. Simulations demonstrate significant improvements in target detection and reduced normalized mean square error in radar channel estimation compared to existing benchmarks.**

***Keywords* — Digital low-resolution radar, adaptive thresholding, environment-aware dithering, one-bit compressive sensing, situation aware sensing**

I. Introduction

Digital radar architectures enable flexible waveform design [1] and strong interference rejection [2]. However, their reliance on high-resolution analog-to-digital converters (ADCs) increases power consumption, hardware complexity, and the amount of data to be processed [3]. These constraints are particularly restrictive in automotive applications, where real-time processing and energy efficiency are critical. To mitigate these issues, low-resolution ADCs—especially one-bit ADCs—have been explored in radar systems [4]–[10]. While one-bit ADCs significantly reduce power consumption and implementation cost, they exhibit poor dynamic range. This is because the quantized received signal is primarily influenced by high radar cross section (RCS) targets, leading to a masking effect that severely degrades the detection of low-RCS targets [11].

Dithering techniques can address dynamic range limitations by introducing time-varying quantization thresholds. Existing methods rely on random dithering [12], second-order statistics target parameters [13], or optimization-based designs [14]–[16]. Sparse recovery-based methods for multiple-input multiple-output (MIMO) radars with few-bit ADCs have shown promise [11], but their performance degrades for closely spaced targets or targets with significant variation in RCS. Recent work has investigated mixed-ADC MIMO radars to address the power consumption issue with high-resolution radars. For instance, [17] employs a combination of high-precision and one-bit ADCs along the spatial dimension. The resolution of the ADCs were fixed along the time dimension in [17]. In contrast, we propose to dynamically adapt ADC resolution over the slow-time dimension. This adaptation allows our method to leverage high-resolution measurements and generate a situation-aware dither signal. Our proposed approach mitigates the masking effect caused by dominant targets, enhancing low-RCS target detection while maintaining low power consumption.

The proposed framework in this paper employs high-resolution ADCs (e.g., 16-bit) in the first slow-time slot, followed by one-bit quantization in subsequent slots within the coherent processing interval (CPI). Depending on the type of ADC circuit, the slow-time resolution adaptation can be achieved by dynamically tuning the ADC parameters [18], changing the oversampling rate in a Σ-Δ ADC [19], or introducing switches within a successive approximation register ADC [20]. The high-resolution measurements are used to estimate the range and RCS of dominant targets. This information, along with Doppler statistics, is used to generate a situation-aware dither signal. In this paper, we show how our generated dither signal mitigates the masking effect of strong targets, enhancing the detection of weaker ones. We develop a three-stage radar channel estimation method which comprises these steps: (1) Extracting dominant target features (i.e., range and RCS) for dither signal construction, (2) Estimating the radar channel from dithered low-resolution measurements, and (3) Compensating for scaling ambiguity caused by heavy quantization. We demonstrate through simulations that our approach improves the detection of low-RCS targets and reduces the normalized mean square error (NMSE) of the estimated radar channel compared to existing benchmarks.

In this paper, we consider a single antenna receiver and focus on range-Doppler radar channel estimation. Further, we assume that the maximum number of targets in any range bin is one, i.e., it is not possible to observe targets at $10\,\mathrm{m}$ with two different Doppler values. In practice, this assumption can be justified when the radar has sufficient range resolution and can isolate returns from each direction by employing beamforming. We also consider the extreme case of one-bit for low-resolution quantization. Our framework, however, can

This work was supported in part by the Dutch Ministry of Economic Affairs and in part by the Important Projects of Common European Interest (IPCEI) Microelectronics and Communication Technology (ME/CT) Project.

2025 IEEE Radar Conference (RadarConf25) | 979-8-3315-4433-1/25/$31.00 ©2025 IEEE | DOI: 10.1109/RADARCONF2559087.2025.11205063

be directly applied to radars using few-bit ADCs by using the appropriate likelihood function in our objective.

Notation: Scalars (e.g., x) are denoted in italic, deterministic vectors (e.g., $\boldsymbol{x}$) in italic bold, matrices (e.g., $\boldsymbol{X}$) in italic bold capital, random variables (e.g., x) in upright, random vectors (e.g., $\mathbf{x}$) in bold upright, and random matrices (e.g., $\mathbf{X}$) in bold capital upright letters. The Hadamard product is denoted by $\odot$ and the Kronecker product by $\otimes$. The transpose is denoted by $(\cdot)^T$. Also, $\Re(\cdot)$ returns the real and $\Im(\cdot)$ the imaginary part.

II. Signal Model

We consider a single-input single-output digital radar. The transmitted signal is constructed by periodically repeating the N-length digital sequence

$$\boldsymbol{s} = \begin{bmatrix} s(0) & s(1) & \cdots & s(N-1) \end{bmatrix}^T. \tag{1}$$

We define T_s as the chip duration and $T_\mathrm{p} = NT_\mathrm{s}$ as the pulse repetition interval (PRI). The L slow-time slots within each CPI are indexed by $\ell \in \{0, 1, \cdots, L-1\}$. Our receiver uses an infinite resolution at the ADC in the first slow-time slot ($\ell = 0$) and one-bit resolution in the remaining $L-1$ slots ($1 \le \ell \le L-1$). The use of infinite resolution enables generating a situation-aware dithering signal, while a one-bit resolution ensures that the power consumption is low. In this section, we discuss the system model for one-bit measurements acquired using a generic dither signal. In Section III, we detail the construction of our dither signal using high-resolution measurements from the first slow-time slot.

For the signalling structure Fig. 1a, the baseband representation of the transmitted signal can be written as

$$s_{\mathrm{TX}}(t) = \sum_{\ell=-\infty}^{\infty} \sum_{n=0}^{N-1} s(n) p(t - nT_\mathrm{s} - \ell T_\mathrm{p}), \tag{2}$$

where $p(t)$ is a rectangular pulse of duration T_s (unity for $0 \le t \le T_\mathrm{s}$ and zero otherwise). We partition the range and Doppler domains into N_r ($N_\mathrm{r} \le N$) and N_d discrete bins, with bin indices denoted by n_r and n_d respectively. The received signal is then

$$z(t) = \sum_{n_\mathrm{r}=1}^{N_\mathrm{r}} \sum_{n_\mathrm{d}=1}^{N_\mathrm{d}} \gamma_{n_\mathrm{r} n_\mathrm{d}} s_{\mathrm{TX}}(t - \tau_{n_\mathrm{r}}) e^{j2\pi f_{n_\mathrm{d}} t} + e(t), \tag{3}$$

where $\tau_{n_\mathrm{r}} = n_\mathrm{r} T_\mathrm{s}$ denotes time delay, f_{n_d} denotes Doppler shift, $\gamma_{n_\mathrm{r} n_\mathrm{d}}$ denotes the reflection coefficient of the target in the $(n_\mathrm{r}, n_\mathrm{d})$-th bin, and $e(t)$ is additive noise.

We ignore the phase variation due to Doppler within a PRI. Under this assumption, the received baseband signal in (3) for the ℓth slow-time slot is

$$z_\ell(t) = \sum_{n_\mathrm{r}, n_\mathrm{d}} \sum_{n=0}^{N-1} \gamma_{n_\mathrm{r} n_\mathrm{d}} s((n + n_\mathrm{r}) \bmod N) \, p(t - (n_\mathrm{r} + n)T_\mathrm{s}) e^{j2\pi \nu_{n_\mathrm{d}} \ell} + e(t), \tag{4}$$

where $\nu_{n_\mathrm{d}} = f_{n_\mathrm{d}} T_\mathrm{p}$, and $((n + n_\mathrm{r}) \bmod N)$ is the remainder when $(n + n_\mathrm{r})$ is divided by N. The discrete-time representation

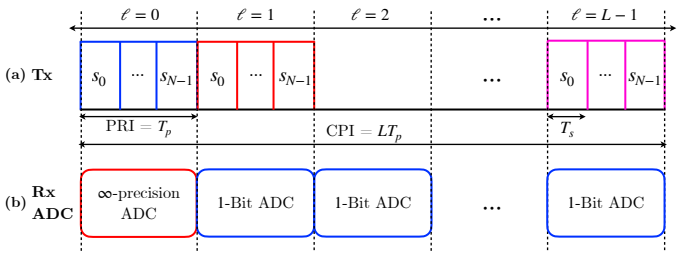

Fig. 1. Transmit signal and resolution at the receiver ADC. We consider a digital radar transmitter that periodically transmits sequence $\boldsymbol{s}$ every PRI. A sketch of this signal is shown in (a). The receiver uses an ADC whose resolution can be adapted in slow-time, as shown in (b). In this paper, the ADC's resolution is set high only during the first slow-time slot of each CPI.

of $z_\ell(t)$ at the N time instances in $\{\ell T_\mathrm{p}, \cdots, \ell T_\mathrm{p} + (N-1)T_\mathrm{s}\}$ is then

$$\boldsymbol{z}_\ell = \boldsymbol{S}\boldsymbol{\Gamma}\boldsymbol{a}_\ell + \boldsymbol{e}_\ell, \tag{5}$$

where $\boldsymbol{\Gamma} \in \mathbb{C}^{N_\mathrm{r} \times N_\mathrm{d}}$ is the reflection coefficient matrix, where $\boldsymbol{\Gamma}(n_\mathrm{r}, n_\mathrm{d}) = \gamma_{n_\mathrm{r}, n_\mathrm{d}}$ denotes the effective RCS of the $(n_\mathrm{r}, n_\mathrm{d})$-th range-Doppler bin. The matrix $\boldsymbol{S} \in \mathbb{C}^{N \times N_\mathrm{r}}$ has its n_r-th column as $s((n + n_\mathrm{r}) \bmod N)$. The steering vector $\boldsymbol{a}_\ell$ is defined as

$$\boldsymbol{a}_\ell = \begin{bmatrix} e^{j2\pi\nu_1\ell}, e^{j2\pi\nu_2\ell}, \cdots, e^{j2\pi\nu_{N_\mathrm{d}}\ell} \end{bmatrix}^T. \tag{6}$$

The signal received in the first slow-time slot in the proposed framework is unquantized, i.e., the receiver acquires $\boldsymbol{z}_0$ as shown in Fig. 1b. The remaining $L-1$ vectors corresponding to the subsequent slow-time slots, i.e., $\{\boldsymbol{z}_\ell\}_{\ell=1}^{L-1}$, are quantized to one-bit. To construct the one-bit measurement model, we first write the collection of unquantized vectors as

$$\boldsymbol{Z} = [\boldsymbol{z}_1, \boldsymbol{z}_2, \cdots, \boldsymbol{z}_{L-1}] = \boldsymbol{S}\boldsymbol{\Gamma}\boldsymbol{A} + \boldsymbol{E}, \tag{7}$$

where $\boldsymbol{A} = [\boldsymbol{a}_1, \boldsymbol{a}_2, \cdots, \boldsymbol{a}_{L-1}]$ is a Vandermonde matrix and $\boldsymbol{E} = [\boldsymbol{e}_1, \boldsymbol{e}_2, \cdots, \boldsymbol{e}_{L-1}]$ is the noise matrix. By vectorizing $\boldsymbol{\Gamma}$ as $\boldsymbol{\gamma} = \mathrm{vec}(\boldsymbol{\Gamma})$, and similarly defining $\boldsymbol{z} = \mathrm{vec}(\boldsymbol{Z})$ and $\boldsymbol{e} = \mathrm{vec}(\boldsymbol{E})$, we obtain

$$\boldsymbol{z} = \boldsymbol{B}\boldsymbol{\gamma} + \boldsymbol{e}, \quad \boldsymbol{B} = \boldsymbol{A}^T \otimes \boldsymbol{S}. \tag{8}$$

The vector $\boldsymbol{z}$ is first dithered, equivalently subtracted, using a discrete-time representation of a known analog dither signal $\boldsymbol{q}(t)$. We denote $\boldsymbol{q} = \boldsymbol{q}_\Re + j\boldsymbol{q}_\Im$ as the discrete-time version of $\boldsymbol{q}(t)$ and write the dithered signal as $\boldsymbol{z} - \boldsymbol{q}$. The dithered signal is finally quantized using a one-bit ADC to output

$$\boldsymbol{y}_\Re = \mathrm{sign}(\Re[\boldsymbol{z}] - \boldsymbol{q}_\Re), \qquad \boldsymbol{y}_\Im = \mathrm{sign}(\Im[\boldsymbol{z}] - \boldsymbol{q}_\Im), \tag{9}$$

where $\mathrm{sign}(\cdot)$ denotes the sign function which is -1 for negative arguments and $+1$ otherwise. The complex measurement vector $\boldsymbol{y}$ can then be written as

$$\boldsymbol{y} = \boldsymbol{y}_\Re + j\boldsymbol{y}_\Im. \tag{10}$$

In automotive radar applications, the range-Doppler channel $\boldsymbol{\Gamma}$ is sparse due to unoccupied cells in the high-dimensional range-Doppler grid and high-frequency scattering. This sparsity enables compressed sensing (CS)-based techniques to

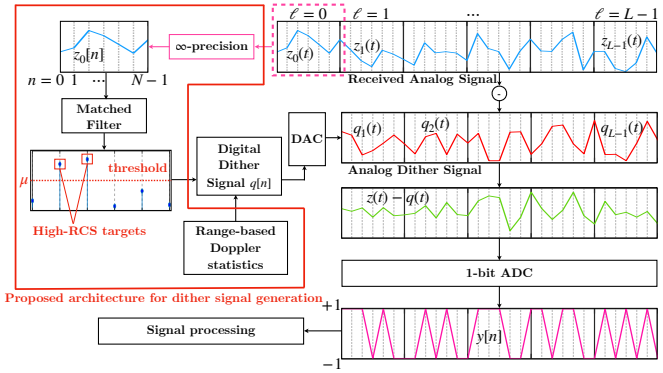

Fig. 2. A matched filter is applied over the high-resolution measurements from the first slow-time slot to detect high-RCS targets. The range and RCS estimates of these targets, together with the Doppler statistics, are used to generate a dither signal. One-bit measurements are acquired in the subsequent slow-time slots using the generated dither signal.

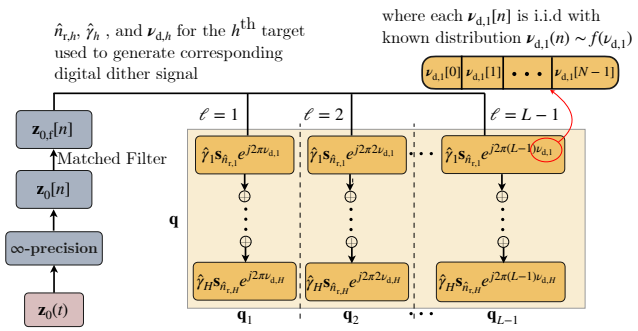

Fig. 3. For H identified high-RCS targets, the dither signal in our method is obtained by adding dithers for each high-RCS target using their Doppler statistics.

efficiently reconstruct the radar channel by leveraging sparse priors.

III. Proposed Method

In this section, we discuss our receiver architecture which alleviates the masking effect induced by high-RCS targets on low-RCS targets in one-bit sparse recovery. The key idea underlying our approach is to "predict" future returns from high-RCS targets using high-resolution measurements from the first slow-time slot ($\ell = 0$) and Doppler statistics. The predictions, in the form of dither signals, are subtracted from the received analog returns for $1 \leq \ell \leq L-1$ before one-bit quantization. A schematic of the proposed receiver architecture is shown in Fig. 2.

A. Proposed dither signal generation

Without loss of generality, assume H high-RCS targets are detected after matched filtering at $\ell = 0$. Given the detected range and lane topology, the Doppler shift distributions of these targets can be inferred. For example, a target detected $18\,\text{m}$ away from the ego vehicle along $60°$ in Fig. 6 occurs on the lane where the speed limit is $80 - 100$ kmph. The probability distribution of the Doppler of targets on this lane can be learned from a history of radar scans or from the infrastructure. In this paper, we assume that this distribution is known. Using this Doppler information, future returns from high-RCS targets within a CPI can be "predicted". Our prediction is a randomized dither signal due to the uncertainty in Doppler information (e.g. $80 - 100$ kmph). We will show that the constructed randomized dither signal achieves better radar channel reconstruction than comparable methods.

To construct the dither signal, our approach first estimates target range and RCS from high-resolution ADC measurements in the first slow-time slot ($\ell = 0$), as shown in Fig. 2. The resulting high-precision signal $\boldsymbol{z}_0[n]$ is matched-filtered to yield $\boldsymbol{z}_{0,\text{f}}[n]$, from which high-RCS targets are identified using a threshold μ, i.e., $\{n : |\boldsymbol{z}_{0,\text{f}}[n]| > \mu\}$. Denoting the estimated RCS and range bin of the h-th target as $\hat{\gamma}_h$ and $\hat{n}_{\text{r},h}$, respectively, the expected return at slow-time slot ℓ from all high-RCS targets can be expressed as the sum of the individual target returns. Consequently, the resulting dither signal $\boldsymbol{q}_\ell[n]$ is given by

$$\boldsymbol{q}_\ell[n] = \sum_{h=1}^{H} \hat{\gamma}_h \boldsymbol{s}_{\hat{n}_{\text{r},h}}[n] e^{j2\pi \nu_{\text{d},h}[n]\ell}, \tag{11}$$

where $\boldsymbol{s}_{\hat{n}_{\text{r},h}}$ is the circularly shifted transmit sequence. Since the Doppler shift $\boldsymbol{\nu}_{\text{d},h}[n]$ is unknown, we sample it at random from its known distribution $f(\boldsymbol{\nu}_h)$ in each fast-time interval. The dither vector shown in Fig. 3 is then constructed as

$$\boldsymbol{q} = [\boldsymbol{q}_1, \boldsymbol{q}_2, \cdots, \boldsymbol{q}_{L-1}]. \tag{12}$$

This dither signal is used, in the form of an analog cancellation signal, to acquire one-bit measurements of the radar channel using (9).

The one-bit measurements acquired with the dither signal $\boldsymbol{q}$ can now be used to estimate the range-Doppler radar channel. However, this estimate is coarse due to two factors: (i) dithering attenuates high-RCS target returns, reducing their reflection coefficients and unmasking low-RCS targets, and (ii) one-bit sparse recovery introduces a scaling ambiguity, as $\text{sign}(az) = \text{sign}(z)$ for any $a > 0$. To address these issues, we propose a two-step approach to separately estimate the reflection coefficients of high- and low-RCS targets.

B. Channel Estimation with Mixed-Resolution Measurements

We use $\hat{\boldsymbol{\gamma}}_{\text{ob}} \in \mathbb{C}^{N_\text{r} N_\text{d}}$ to denote the sparse vector estimated from one-bit measurements. This estimate can be obtained from any one-bit CS algorithm such as [12]. Its corresponding range-Doppler representation, denoted by $\hat{\boldsymbol{\Gamma}}_{\text{ob}} \in \mathbb{C}^{N\text{r} \times N_\text{d}}$, is obtained by reshaping $\hat{\boldsymbol{\gamma}}_{\text{ob}}$ into a matrix. Given our assumption of at most one target per range bin, false-alarms are suppressed by retaining only the strongest coefficient in each row. To mask the false-alarms, we define a binary matrix $\mathbf{M}_{\text{ob}} \in \{0,1\}^{N_\text{r} \times N_\text{d}}$ as

$$\mathbf{M}_{\text{ob}}[i,j] = \begin{cases} 1, & j = \underset{k}{\text{argmax}}\ |\hat{\boldsymbol{\Gamma}}_{\text{ob}}[i,k]|, \\ 0, & \text{otherwise.} \end{cases}$$

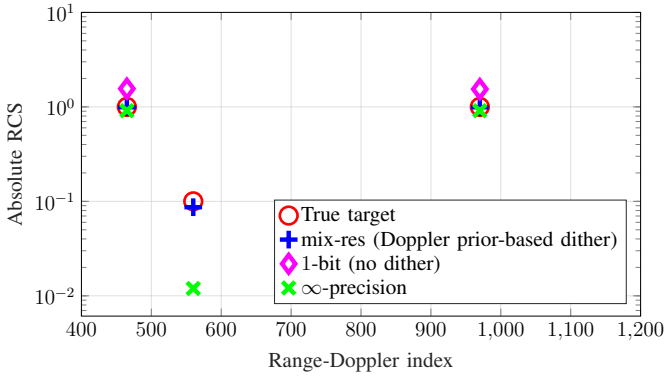

Fig. 4. Channel estimation for two high-RCS targets with Doppler prior of length 4 and $|\gamma| = 1$ each and one low-RCS target with $|\gamma| = 0.1$.

The masked channel estimate is then given by

$$\hat{\mathbf{\Gamma}}_{\text{ob, filt}} = \mathbf{M}_{\text{ob}} \odot \hat{\mathbf{\Gamma}}_{\text{ob}}.$$

We can separate the masked channel $\hat{\mathbf{\Gamma}}_{\text{ob, filt}}$ into high-RCS and low-RCS channels, as high-RCS target parameters are already estimated using the matched filter output $\boldsymbol{z}_{0,\text{f}}[n]$ at $\ell = 0$, with Doppler determined from $\hat{\mathbf{\Gamma}}_{\text{ob, filt}}$ by

$$\hat{n}_{d,h} = \underset{k}{\text{argmax}}\, \mathbf{\Gamma}_{\text{ob, filt}}(\hat{n}_{r,h}, k).$$

The radar channel matrix corresponding to high RCS targets, defined by $\hat{\mathbf{\Gamma}}_{\text{high}}$, is zero everywhere except at these identified locations

$$\hat{\mathbf{\Gamma}}_{\text{high}}(\hat{n}_{r,h}, \hat{n}_{d,h}) = \hat{\gamma}_h. \tag{13}$$

The radar channel matrix associated with low-RCS targets can then be estimated from $\hat{\mathbf{\Gamma}}_{\text{ob, filt}}$ by masking high-RCS targets

$$\hat{\mathbf{\Gamma}}_{\text{low,SA}} = (\mathbf{M}_{\text{ob}} - \mathbf{M}_{\text{high}}) \odot \hat{\mathbf{\Gamma}}_{\text{ob, filt}}, \tag{14}$$

where $\mathbf{M}_{\text{high}}$ is a binary mask identifying high-RCS targets. Due to one-bit recovery, $\hat{\mathbf{\Gamma}}_{\text{low,SA}}$ is accurate only up to a positive scaling factor. We resolve this by isolating the high-resolution low-RCS returns

$$\boldsymbol{y}_{0,\text{low}} = \boldsymbol{y}_0 - \boldsymbol{S}\hat{\mathbf{\Gamma}}_{\text{high}}\boldsymbol{a}_0.$$

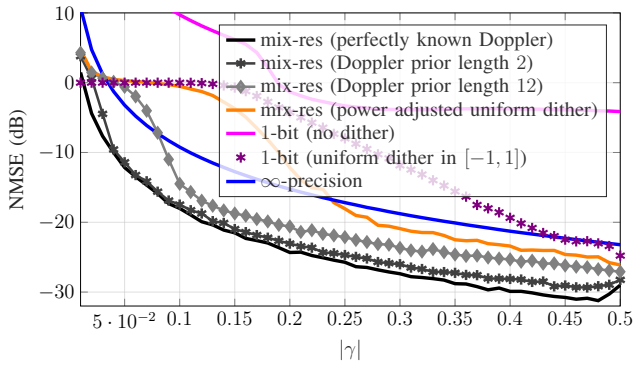

Fig. 5. Comparison of NMSE in the estimated RCS of the weak target in the presence of two dominant targets for a grid size $N \times L = 40 \times 40$ for different dithering signals and receiver designs.

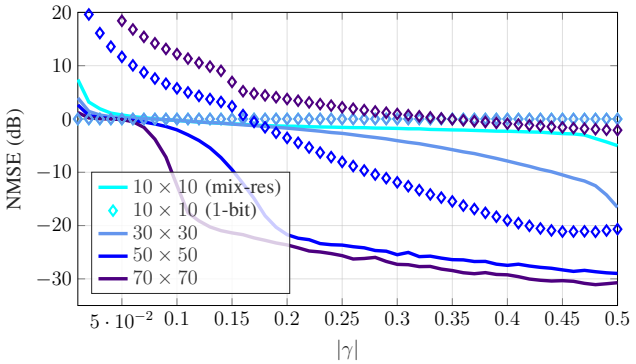

Fig. 6. Comparison of NMSE in the estimated RCS of the weak target in the presence of two dominant targets for different grid sizes $N \times L$ for proposed mixed-resolution system architecture and Doppler prior length 4.

The expected low-RCS returns are given by $\delta \boldsymbol{S}\hat{\mathbf{\Gamma}}_{\text{low,SA}}\boldsymbol{a}_0$, where $\delta > 0$ is unknown and estimated as

$$\hat{\delta} = \underset{\delta}{\text{argmin}} \|\boldsymbol{y}_{0,\text{low}} - \delta \boldsymbol{S}\hat{\mathbf{\Gamma}}_{\text{low,SA}}\boldsymbol{a}_0\|_2^2.$$

The final low-RCS channel estimate is

$$\hat{\mathbf{\Gamma}}_{\text{low}} = \hat{\delta}\hat{\mathbf{\Gamma}}_{\text{low,SA}}. \tag{15}$$

Thus, the complete range-Doppler channel estimate is given by

$$\hat{\boldsymbol{\gamma}} = \text{vec}(\hat{\mathbf{\Gamma}}_{\text{low}} + \hat{\mathbf{\Gamma}}_{\text{high}}),$$

where $\hat{\boldsymbol{\gamma}}$ includes reflection coefficients of both the high- and low-RCS targets.

IV. Results and Discussion

We consider a two-target scenario to analyze the accuracy of detecting the low-RCS target as a function of the dynamic range. Fig. 4 simulates an 80 GHz radar channel with two high-RCS targets ($|\gamma| = 1$) and one low-RCS target ($|\gamma| = 0.1$). The Doppler of high-RCS targets follows a uniform distribution over four values, $\nu_H \sim \mathcal{U}\{0.08, 0.18, 0.28, 0.38\}$, with actual

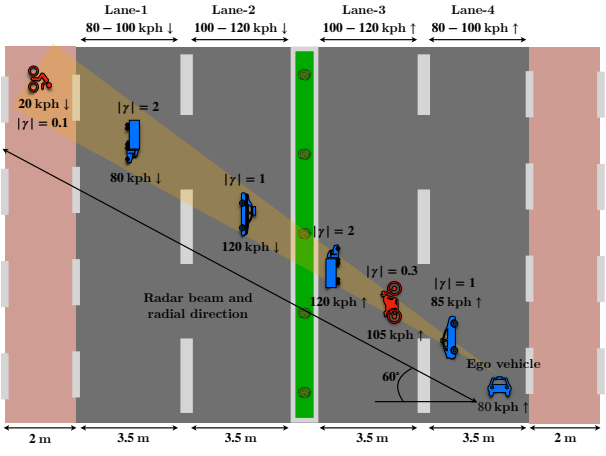

Fig. 7. Multi-lane highway scenario with targets of varying velocities and RCS values. We assume that the radar can isolate returns from any direction by beamforming.

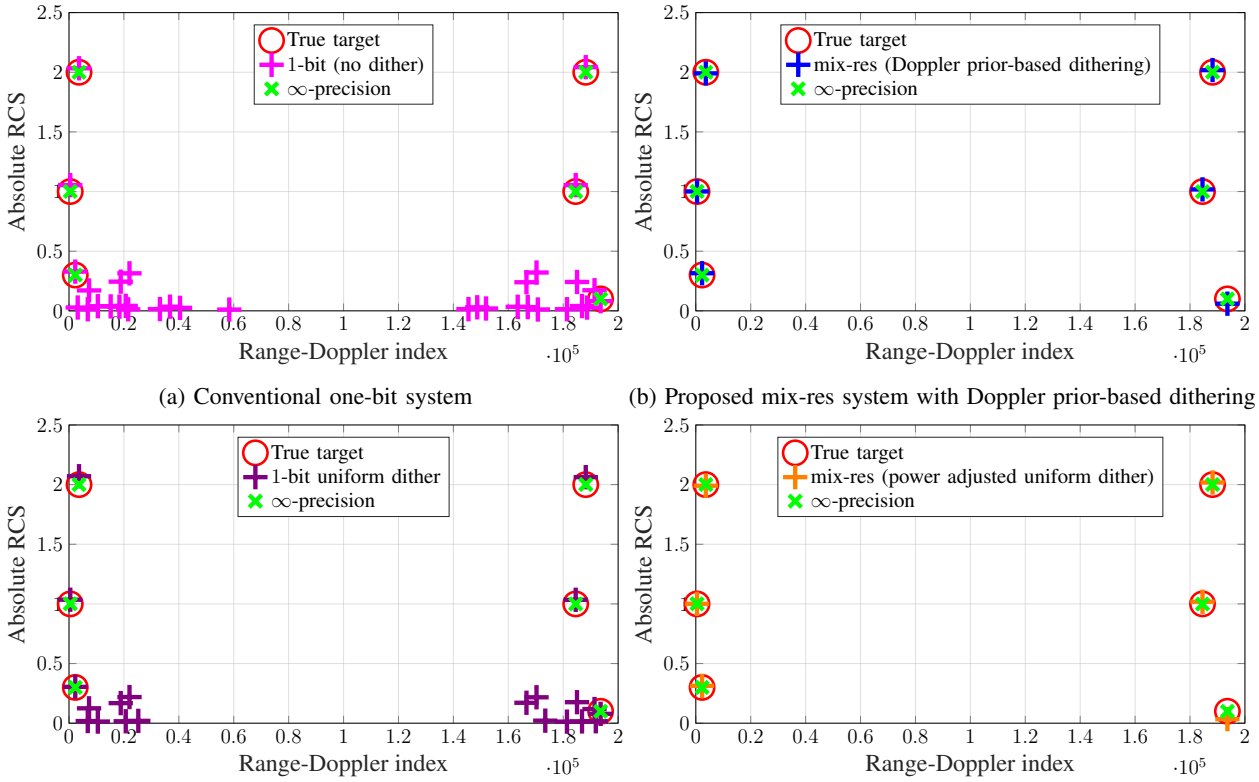

(a) Conventional one-bit system

(b) Proposed mix-res system with Doppler prior-based dithering

(c) Conventional one-bit system with uniform dithering

(d) Mix-res system with power adjusted uniform dithering

Fig. 8. Channel estimation results for the multi-lane highway scenario in Fig. 7 with different dithering signals and receiver designs. The proposed situation-aware dithering technique with a mixed-resolution ADC detects both high- and low- RCS targets, while a conventional one-bit system fails in detecting the low-RCS targets.

Doppler shifts of 0.28 and 0.38. We simulate for range resolution of 1m, Chip duration of 6.67ns, and badwidth of 5GHz. The radar channel is estimated via log-likelihood minimization [12] with a log-sum sparsity penalty [21]. Despite Doppler ambiguities, Fig. 4 demonstrates that the proposed method effectively suppresses high-RCS responses, enabling low-RCS target detection.

Note: Doppler prior length is defined as the number of possible Doppler shifts for a high-RCS target (e.g., 4 in Fig. 4). Doppler priors are assumed uniform within lane-based limits. For example, a prior length of 2 with a Doppler range $\{\nu_{\mathrm{a}}, \nu_{\mathrm{b}}\}$ implies $\nu \sim \mathcal{U}\{\nu_{\mathrm{a}}, \nu_{\mathrm{b}}\}$.

To assess performance, we evaluate the NMSE of the radar channel associated with the low-RCS targets, i.e.,

$$\mathrm{NMSE} = 10\log_{10}\frac{\|\mathbf{\Gamma}_{\text{true}} \odot (\mathbf{M}_{\text{ob}} - \mathbf{M}_{\text{high}}) - \hat{\mathbf{\Gamma}}_{\text{low}}\|_2^2}{\|\mathbf{\Gamma}_{\text{true}} \odot (\mathbf{M}_{\text{ob}} - \mathbf{M}_{\text{high}})\|_2^2}$$

where $\mathbf{\Gamma}_{\text{true}}$ is the ground truth range-Doppler matrix.

The NMSE in Fig. 5 and Fig. 6 is averaged over 1000 trials with independently generated dither signals. The low-RCS target strength is varied from 0.01 to 0.5 to analyze detection robustness. In addition to the zero thresholding in one-bit, we compare our method against two uniform random dithering techniques:

a) Uniform Random Dithering [12]: One-bit quantization is applied across all slow-time slots. The dither signal for each pair of ℓ and n is drawn from i.i.d uniform distribution, i.e., $\tilde{\boldsymbol{q}}_\ell[n] \sim \mathcal{U}[-1, 1]$.

b) Power-Adjusted Uniform Random Dithering: Our method uses high-resolution ADCs in the first slow-time slot, unlike [12], which employs one-bit ADCs throughout. For a fair comparison, we adapt [12] to our ADC resolution profile by estimating high-RCS target power, p_H, from the matched filter output.

A dither signal with entries drawn from $\mathcal{U}[-1, 1]$ is effective when the power of high-RCS targets is comparable to the dither signal's power, i.e., $1/3$. This is because the average power of $\mathcal{U}[-1, 1]$ is $1/3$. When the power p_H is substantially different from $1/3$, the uniform dithering technique becomes less effective. The power-adjusted uniform random dithering benchmark generates a dither signal whose power is comparable to p_H. This is achieved by drawing the dither signal entries according to $\boldsymbol{q}_\ell[n] \sim \mathcal{U}\left[-\sqrt{3p_H}, \sqrt{3p_H}\right]$. The choice of the limits $-\sqrt{3p_H}$ and $\sqrt{3p_H}$ ensures that the average power of the dither signal matches the high-RCS signal power p_H.

Fig. 5 presents NMSE results with $N = L = 40$, using a Doppler prior length of 4 per high-RCS target. The proposed mixed-resolution approach outperforms conventional one-bit systems with zero and uniform dithering, as well as power-adjusted uniform dithering. Even with two high-RCS targets, our Doppler prior-based method enables more accurate low-RCS target estimation. Fig. 6 further illustrates that the

proposed method outperforms the benchmarks while requiring fewer measurements than other dithering techniques.

A. Lane Topology-based priors

Fig. 7 illustrates a multi-lane highway scenario, where an ego vehicle with a radar, traveling at $80\,\text{kmph}$, detects multiple targets with the radar beam directed at a 60° angle.

We demonstrate this scenario to emphasize the effectiveness of estimating channel parameters for weak targets in the presence of dominant reflections from high-RCS targets, particularly under conditions with varying Doppler priors. Using the lane topology in Fig. 7, the Doppler priors are assigned based on the range estimates from matched filtering.

The channel estimation results demonstrate the robustness of the proposed mixed-resolution architecture in such complex conditions. The cyclist, with $|\gamma| = 0.1$, represents a low-RCS target with a weak return signal, which is particularly challenging to detect amidst strong reflections from high-RCS targets such as trucks and cars. With $N \times L = 450 \times 450$, conventional one-bit radar systems can detect the cyclist and similar weak targets. However, as seen in Fig. 8a, the one-bit system introduces significant false artifacts around the actual low-RCS targets due to its limited dynamic range. The use of uniformly distributed thresholds reduces these artifacts, but the issue of false alarms persists as seen in Fig. 8c.

Figs. 8b and 8d showcase the channel estimation results obtained using the proposed mixed-resolution architecture with Doppler-prior-based thresholds and power-adjusted uniformly distributed thresholds, respectively. The results clearly highlight the robustness of the mixed-resolution system. Our Doppler-prior-based dithering not only accurately estimates the weak targets but also minimizes false alarms significantly, even in the presence of strong reflections from high-RCS targets. In contrast, while the power-adjusted uniformly distributed thresholds show improvement over conventional one-bit systems, their performance deteriorates as the grid size decreases, consistent with earlier observations. Although the Doppler priors are fixed in our simulations, they can vary across radar frames in practice due to changes in lane topology, allowing the dither to be adapted accordingly.

V. Conclusions

We demonstrated the adaptation of ADC resolution, combined with situation-aware dithering, to effectively increase the dynamic range of low-resolution radars. Our approach configures the ADC to operate at high resolution during the first slow-time slot and at low resolution in the subsequent slots within a CPI. The high-resolution measurements from the initial slot, along with Doppler statistics, are leveraged to generate a dither signal for obtaining low-resolution measurements. Additionally, we developed a radar channel estimation algorithm tailored for these mixed-resolution measurements. Through simulations, we showed that our mixed-resolution framework with situation-aware dithering enhances the detection of low-RCS targets while also achieving lower NMSE in channel estimation compared to existing benchmarks.

References

[1] C. Waldschmidt, J. Hasch, and W. Menzel, "Automotive radar—from first efforts to future systems," *IEEE J. Microw.*, vol. 1, no. 1, pp. 135–148, 2021.

[2] F. Roos, J. Bechter, C. Knill, B. Schweizer, and C. Waldschmidt, "Radar sensors for autonomous driving: Modulation schemes and interference mitigation," *IEEE Microw. Mag.*, vol. 20, no. 9, pp. 58–72, 2019.

[3] R. H. Walden, "Analog-to-digital converter survey and analysis," *IEEE J. Sel. Areas Commun.*, vol. 17, no. 4, pp. 539–550, 1999.

[4] K. U. Mazher, A. Mezghani, and R. W. Heath, "Low resolution millimeter wave radar: Bounds and performance," in *2018 52nd Asilomar Conf. Signals, Syst., Comput.* IEEE, 2018, pp. 554–558.

[5] Z. Cheng, Z. He, and B. Liao, "Target detection performance of collocated MIMO radar with one-bit ADCs," *IEEE Signal Process. Lett.*, vol. 26, no. 12, pp. 1832–1836, 2019.

[6] B. Jin, J. Zhu, Q. Wu, Y. Zhang, and Z. Xu, "One-bit LFMCW radar: Spectrum analysis and target detection," *IEEE Trans. Aerosp. Electron. Syst.*, vol. 56, no. 4, pp. 2732–2750, 2020.

[7] Y. Cheng, X. Shang, and F. Liu, "CRB analysis for mixed-ADC PMCW MIMO radar," in *2021 CIE Int. Conf. Radar*. IEEE, 2021, pp. 1032–1037.

[8] M. Deng, Z. Cheng, L. Wu, B. Shankar, and Z. He, "One-bit ADCs/DACs based MIMO radar: Performance analysis and joint design," *IEEE Trans. Signal Process.*, vol. 70, pp. 2609–2624, 2022.

[9] Y.-H. Xiao, D. Ramírez, P. J. Schreier, C. Qian, and L. Huang, "One-bit target detection in collocated MIMO radar and performance degradation analysis," *IEEE Trans. Veh. Technol.*, vol. 71, no. 9, pp. 9363–9374, 2022.

[10] M. Deng, H. Wu, Z. Cheng, J. Wang, and Z. He, "Matched filtering performance analysis for massive MIMO radar with one-bit quantization," in *2023 IEEE Radar Conf.* IEEE, 2023, pp. 1–6.

[11] C.-Y. Wu, T. Zhang, J. Li, and T. F. Wong, "Parameter estimation in PMCW MIMO radar systems with few-bit quantized observations," *IEEE Trans. Signal Process.*, vol. 70, pp. 810–821, 2022.

[12] X. Shang, H. Zhu, and J. Li, "Range-doppler imaging via one-bit PMCW radar," in *2020 IEEE 11th Sensor Array and Multichannel Signal Processing Workshop (SAM)*. IEEE, 2020, pp. 1–5.

[13] A. Ameri, A. Bose, J. Li, and M. Soltanalian, "One-bit radar processing with time-varying sampling thresholds," *IEEE Trans. Signal Process.*, vol. 67, no. 20, pp. 5297–5308, 2019.

[14] F. Foroozmehr, M. Modarres-Hashemi, and M. M. Naghsh, "Transmit code and receive filter design for PMCW radars in the presence of one-bit ADC," *IEEE Trans. Aerosp. Electron. Syst.*, vol. 58, no. 4, pp. 3078–3089, 2022.

[15] B. Wang, H. Li, and Z. Cheng, "Joint transceiver design for massive MIMO DFRC systems with one-bit DACs/ADCs," in *2023 IEEE Globecom Workshops (GC Wkshps)*. IEEE, 2023, pp. 649–654.

[16] F. Foroozmehr, M. Modarres-Hashemi, and M. M. Naghsh, "One-bit PMCW radar: Designing binary transmit code and receive filter via a worst-case approach," *IEEE Trans. Veh. Technol.*, 2024.

[17] X. Shang, R. Lin, and Y. Cheng, "Mixed-ADC based PMCW MIMO radar angle-doppler imaging," *IEEE Trans. Signal Process.*, 2024.

[18] M. Trakimas and S. R. Sonkusale, "An adaptive resolution asynchronous adc architecture for data compression in energy constrained sensing applications," *IEEE Trans. on Circuits and Sys. I: Regular Papers*, vol. 58, no. 5, pp. 921–934, 2010.

[19] R. Stewart and E. Pfann, "Oversampling and sigma-delta strategies for data conversion," *Electron. Commun. Eng. J.*, vol. 10, no. 1, pp. 37–47, 1998.

[20] S. O'Driscoll, K. V. Shenoy, and T. H. Meng, "Adaptive resolution ADC array for an implantable neural sensor," *IEEE Trans. on Biomed. Circuits and Sys.*, vol. 5, no. 2, pp. 120–130, 2011.

[21] J. Fang, F. Wang, Y. Shen, H. Li, and R. S. Blum, "Super-resolution compressed sensing for line spectral estimation: An iterative reweighted approach," *IEEE Trans. Signal Process.*, vol. 64, no. 18, pp. 4649–4662, 2016.